High temperature ferromagnetism and optical properties of Co doped ZnO nanoparticles

Bappaditya Pal and P. K. Giri[a)]

Department of Physics, Centre for Nanotechnology, Indian Institute of Technology, Guwahati 781039, India

We report on the occurrence of high temperature ferromagnetism (FM) in ZnO nanoparticles (NPs) doped with Co-atoms. ZnO NPs of two different initial sizes are doped with 3% and 5% Co using ball milling and FM is studied at room temperature and above. X-ray diffraction and high-resolution transmission electron microscopy analysis confirm the absence of metallic Co clusters or any other phase different from würtzite-type ZnO. UV-visible absorption studies show change in band structure and photoluminescence studies show green emission band at 520 nm indicating incorporation of Co-atoms and presence of oxygen vacancy defects, respectively in ZnO lattice. Micro-Raman studies of doped samples shows defect related additional bands at 547 and 574 cm^{-1}. XRD and Raman spectra provide clear evidence for strain in the doped ZnO NPs. The field dependence of magnetization (M-H curve) measured at room temperature exhibits the clear FM with saturation magnetization (M_s) and coercive field (H_c) of the order of 3–7 emu/g and 260 Oe, respectively. Temperature dependence of magnetization (M-T) measurement shows sharp ferromagnetic to paramagnetic transition with a high Curie temperature (T_c) of ~ 800 K for 3% Co doped ZnO NPs. It is found that doping at 5% and higher concentration does not exhibit a proper magnetic transition. We attempt to fit the observed FM data with the bound magnetic polaron (BMP) model involving localized carriers and magnetic cations. However, calculated concentration of the BMPs is well below the typical percolation threshold in ZnO. We believe that observed high temperature FM is primarily mediated by defects in the strained NPs. ZnO NPs of lower initial size show enhanced FM that may be attributed to size dependent doping effect. © *2010 American Institute of Physics*. [doi:10.1063/1.3500380]

I. INTRODUCTION

Diluted magnetic semiconductors (DMSs), where transition metal (TM) atoms are introduced into the cationic sites of the semiconducting host lattice, have recently attracted increasing attention because of their potential use in spintronic devices.[1–5] Carrier spins are used to transport, store, and process information in novel ways, providing both enhanced performance and new functionalities in order to increase both speed and storage capacity in traditional microelectronic devices.[6,7] The main challenge in the practical applications of the DMS materials is the attainment of ferromagnetism (FM) above room temperature (RT) to be compatible with junction temperatures. In an important development, Dietl *et al.*[3] predicted the existence of high temperature FM in some magnetically doped wide band gap semiconductors that has led to multiple experimental and computational studies of these materials. Much attention has been paid to TMs-doped wide band gap semiconductors (II–VI and III–V). Among II–VI semiconductors, ZnO has been considered as one of the promising candidates for fabricating DMSs due to its high solubility for TMs and superior semiconductor properties. Moreover, ZnO is a wide band gap (3.27 eV) semiconductor with a large exciton binding energy (60 meV) and has potential applications in electronic and optoelectronic devices.[8] Particularly, TM-doped ZnO DMSs

have been extensively investigated since theoretical studies predicted it's Curie temperature (T_c) to be above RT. Recently, origin of FM ordering in pristine mircostructured and nanostructured ZnO has been discussed and role of surface defect was emphasized.[9–11] However, the magnitude of FM in such undoped systems is usually too low for any practical application.

In spite of several studies reported on ZnO-based DMSs, there is no clear agreement about the nature and origin of the magnetic properties of samples prepared by different methods and different groups.[12] It is being currently debated whether the observed FM in oxide DMS has anything to do with TM doping or might be solely related to intrinsic defects.[10,13] Some reports suggested segregation and the formation of Co clusters as the origin of FM signal,[14] but more recent results seems to indicate the existence of intrinsic FM.[15–17] Ueda and Kawai reported FM with a Curie temperature higher than RT for the Co doped ZnO films grown by the pulsed-laser deposition technique.[18] Song *et al.*[19] reported RT FM and a high T_c of 750 K for the Co doped ZnO ferromagnetic films. Deka *et al.*[20] have synthesized polycrystalline $Zn_{1-x}Co_xO$ by a low temperature combustion and found FM in this material up to 750 K. Recently, Jayakumar *et al.*[21] reported Mn-doped ZnO polycrystalline samples synthesized by a surfactant-assisted method showing robust room-temperature FM. Rao and Deepak[22] observed the absence of FM in Co doped ZnO powder fabricated by the low temperature decomposition of acetate solid solution. These

a)Electronic mail: giri@iitg.ernet.in.

108, 084322-1

controversial results between research groups suggest that the magnetic properties of DMS materials seem to be very sensitive to the preparation method and the structure of materials.[9] Here we have doped Co in ZnO NPs by using a mechanical ball milling process and it proves to be an effective and simple technique to prepare TM-doped semiconductors that exhibit high temperature FM.

In this work, we report on the magnetic, structural and optical properties of Co doped ZnO NPs. X-ray diffraction (XRD) and transmission electron microscopy (TEM) are used to examine phase segregation and morphological analysis. Micro Raman scattering and photoluminescence (PL) spectrum are measured to confirm the presence of oxygen vacancy defects. UV-Vis optical absorption is used to infer the substitution of cobalt inside the Zn lattice corresponding to the bandgap shift. Vibrating sample magnetometer (VSM) is employed to measure the RT magnetic properties and the variation in magnetization with temperature. The observed magnetization and its temperature dependence are discussed with reference to the role of defects and doping concentration in the ZnO sublattice.
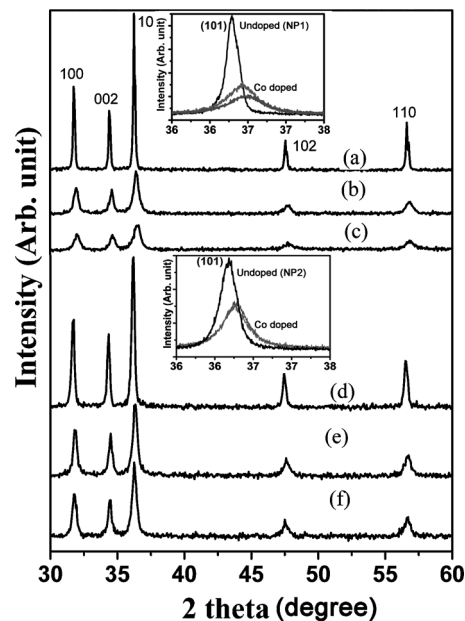

FIG. 1. XRD pattern of the Co doped ZnO NPs. For NP1: (a) undoped, (b) 3% Co doped, (c) 5% Co doped; for NP2: (d) undoped, (e) 3% Co doped, (f) 5% Co doped. The insets show comparison of the (101) peak for undoped and doped ZnO NPs. Peak shift is evident in Co doped NPs in both cases.

II. EXPERIMENTAL DETAILS

The starting materials are commercial ZnO nanopowder (purity 99.999%, Sigma Aldrich) and cobalt (Co) powder (99.5%, Loba Chemie). 3% and 5% Co powders are doped with the ZnO nanopowder of two different initial average sizes 80 nm and 40 nm, named as NP1 and NP2, respectively. After mixing, the powders are ground for 10 min and milled in a mechanical ball milling machine (Retsch, PM 100) at 350 rpm for duration of 5 and 8 h in a zirconium oxide vial under atmospheric pressure and temperature. Zirconium oxide balls of diameter 5 mm are used in this experiment. The ball to powder mixture weight ratio is taken as 10:1. Postgrowth annealing is done for the 5 h milled sample at two different temperatures: 250 and 500 °C for 1 h.

The crystal structures of the obtained samples are characterized by XRD patterns (Bruker D8 Advance, Cu K_α radiation) and micro-Raman spectroscopy (LabRam HR800, Jobin Yvon). Morphology and structures of as-synthesized samples are observed by high-resolution TEM (HRTEM) (JEOL-JEM 2010 operated at 200 keV). Specimens for HR-TEM investigations are prepared by dispersing powder particles in methanol and drop casting it on a carbon coated copper grid of 400 meshes (Pacific Grid, USA). HRTEM imaging and microanalysis by energy-dispersive x-ray spectroscopy (EDS) are conducted in the same microscope. The magnetic properties of the samples are measured by using a Lakeshore (model 7410) VSM. The UV-Vis spectroscopy measurements are recorded using a commercial spectrophotometer (Varian) with a monochromated xenon lamp source. The steady state PL spectrum is recorded at RT by using a 325 nm He–Cd laser excitation coupled in a commercial high-end fluorimeter (Edinburg, FSP920).

III. RESULTS AND DISCUSSION

A. Structural characterization

Figure 1 shows some typical XRD patterns of the Co doped ZnO NPs. Figures 1(a)–1(c) are for undoped, 3% doped, and 5% doped NP1, respectively. Similarly, Figs. 1(d)–1(f) are for undoped, 3% doped, and 5% doped NP2, respectively. For each sample, all the observed diffraction peaks can be indexed to a ZnO wurtzite structure (space group $P6_3mc$), and no other impurity phase was found, which indicates that the Co ions successfully occupy the lattice site rather than interstitial ones. In addition, very slow scans near the peaks of both hexagonal and cubic cobalt phases reveal no signatures of any kind of additional phases in the NPs. XRD Measurement of Co powder shows one intense peak around 44° which does not appear for the doped samples indicating Co is doped well in the ZnO sublattice. Compared to undoped ZnO, the doped samples shows lowering of intensity and increase in full width at half maxima of the XRD pattern. Nanoparticle (NP) size is reduced considerably for the doped samples during milling compared to undoped NPs of two different initial sizes, as shown in Table I. Interestingly, a slow scan comparison of the (101) peak of Co doped and the undoped ZnO NPs show a higher 2θ value and lower intensity for the doped ZnO NPs, as shown in the inset of Fig. 1. The peak shift is larger in case of NP1 as compared to NP2. The change in the XRD pattern in doped samples is attributed to size reduction and lattice strain induced by the ball milling. Since the ionic radius of Co and Zn are very close, Co doping induced strain is expected to be less significant. However, as a result of ball milling, a compressive strain is introduced in the ZnO NPs.[23] From the measured shift in 2θ for (101) plane, we estimate a reduction in interplanar spacing (d_{101}) of ~0.38% for NP1 and it is

TABLE I. ZnO NPs of different initial sizes are Co doped at 3% and 5%: Crystallite size determined from XRD profile; saturation magnetization (M_s), coercive filed (H_c), and remanent magnetization (M_r) are determined from M-H curves; transition temperature (T_c) is determined from differentiated M-T curves. M_0, m_{eff}, χ_m, N are determined from fitting of the M-H curve with BMP model [Eq. (1)].

	Crystallite size (nm)						Fitting parameters extracted from BMP model			
Co doping, ZnO source	Undoped	Doped	M_s (emu/g)	H_c (Gauss)	M_r (emu/g)	T_c (K)	M_0 (emu/g)	$m_{eff} \times 10^{-17}$ (emu)	$\chi_m \times 10^{-5}$ (cgs)	$N \times 10^{18}$ (cm^{-3})
3%, NP1	81.8	21.7	3.95	268	0.42	791	4.47	3.43	1.24	0.732
5%, NP1	81.8	18.1	5.91	263	0.68	$\cdots$	6.40	4.03	0.64	0.890
3%, NP2	42.4	25.2	4.39	244	0.43	819	4.68	3.93	0.01	0.668
5%, NP2	42.4	25.1	7.02	264	0.66	$\cdots$	7.88	3.32	1.57	1.330
3%, NP1 250 °C annealed	81.8	$\cdots$	4.21	250	0.35	$\cdots$	$\cdots$	$\cdots$	$\cdots$	$\cdots$
5%, NP2 post M-T	42.4	$\cdots$	0.59	204	0.09	$\cdots$	$\cdots$	$\cdots$	$\cdots$	$\cdots$

little lower for NP2. This strain in the NPs is expected to influence the electronic properties including band structure of ZnCoO. Note that, one cannot exclude the possibility of formation of other precipitates or clusters small enough not to be detected in XRD measurement.

Figure 2(a) and 2(b) shows low-magnification scanning electron microscopy (SEM) images of the undoped ZnO NPs and Figs. 2(c) and 2(d) shows low-magnification TEM of the 3% Co doped ZnO NPs prepared after 5 h of milling. The micrograph reveals average particle size distribution in the range 80–100 nm for NP1 and 40–50 nm for NP2 before milling. For the doped ZnO, the average size of the NPs is about 20–25 nm for NP1 as well as NP2. Different kinds of
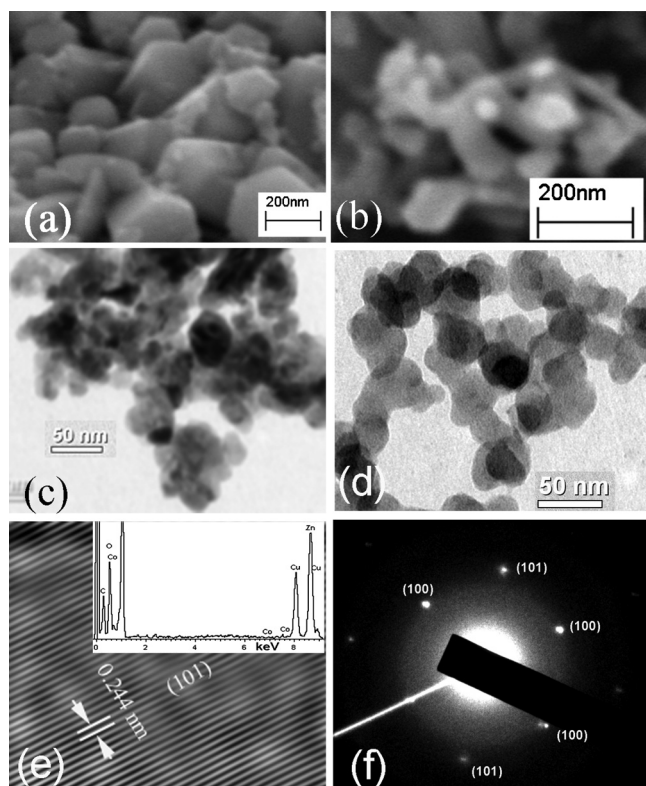

FIG. 2. SEM images of the morphology of the ZnO NPs (a) undoped NP1, (b) undoped NP2. TEM image of the doped (3% Co) NP2: (c) NP1, (d) NP2, (e) HRTEM lattice image of doped NP2 showing no clustering of Co, inset shows EDS spectra showing presence of Co in ZnO NPs, (f) corresponding SAED pattern.

shapes of the NPs are discernible in Figs. 2(a)–2(d): irregularly shaped particle, larger rectangular platelets and hexagonally shaped particles. However, doped NPs are of regular shapes, mostly spherical. HRTEM lattice images are presented in Fig. 2(e), which shows that all the NP2 are single crystalline. The d-spacing of the crystal plane is calculated as 0.244 nm which shows the preferable crystal growth plane is (101) and it is also the highest intensity peak in the XRD pattern shown in Fig. 1. This shows a compressive strain of ~0.81% in the doped ZnO NPs. The crystallinity and preferential orientation of the NPs in the sample are confirmed from the selected area diffraction (SAD) patterns shown in Fig. 2(f), confirming that the ZnCoO NPs are single crystals. The SAD pattern obtained by focusing the beam on a few NPs of the sample clearly indicates the single crystalline nature of each NPs. Also, it confirms that the nanocrystals are indeed in the wurtzite phase. Due to low doping concentration, there is no cobalt clusters observed in the as-prepared NPs. In the EDS spectra measured on few single particle of the as-prepared ZnCoO, Zn, Co, and O related peaks are seen as shown in inset of Fig. 2(e), besides Cu and C peaks from carbon coated Cu grid used in TEM. This indicates that cobalt ions were uniformly distributed in the entire ZnCoO samples.

B. Raman scattering studies

In order to investigate the influence of Co doping on microstructure and vibrational properties, Raman scattering experiments were carried out. Raman scattering is a versatile technique for detecting the incorporation of dopants and the resulted defects and lattice disorder in the host lattice.[24] The zone-center optical phonons of the wurtzite structure of ZnO can be classified according to the following irreducible representations: $\Gamma_{opt} = A_1 + E_1 + 2E_2 + 2B_1$. The B_1 modes are silent in Raman scattering, whereas A_1 and E_1 modes are polar and hence exhibit different frequencies for the transverse-optical (TO) and longitudinal-optical (LO) phonons.[25] The nonpolar E_2 modes have two frequencies, namely, E_2 (high) and E_2 (low) associated with the motion of oxygen (O) atoms and zinc (Zn) sublattice, respectively.[26] Figure 3 shows the room-temperature Raman spectra of undoped and doped samples for NP1 and NP2 in the range 200–800 cm^{-1}. For the undoped ZnO, the sharpest and strongest peak at
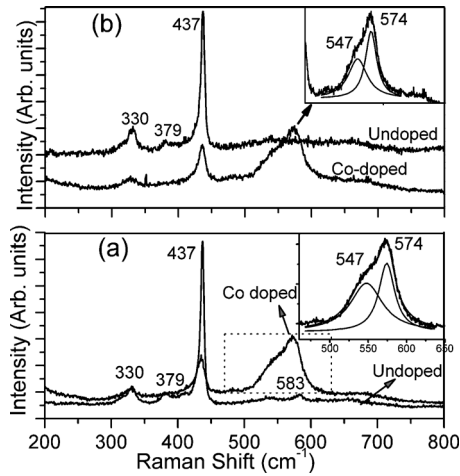
FIG. 3. Raman Spectra for the undoped and 3% Co doped ZnO NPs: (a) NP1 (b) NP2, The inset on the upper right corner in each case shows the magnified view of the defect related Raman bands in the in Co doped samples. The peaks are fitted with Lorentzian line shape.
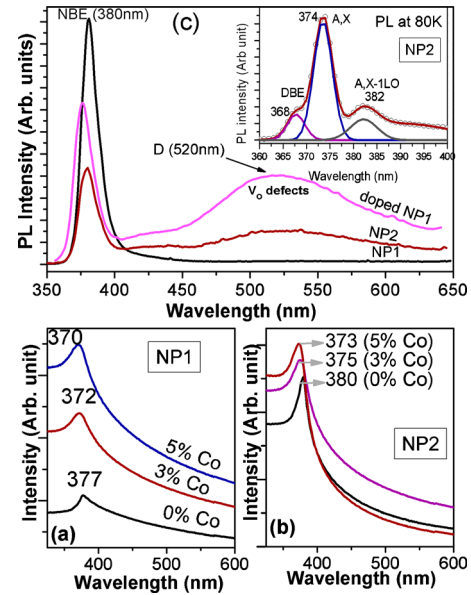

FIG. 4. (Color online) (a) UV-Vis absorption spectra of undoped and Co doped ZnO NPs (3% and 5%) for NP1. and (b) UV-Vis absorption spectra of undoped and Co doped ZnO NPs (3% and 5%) for NP2. Doped NPs shows clear blueshifted band. (c) Comparison of PL spectra of undoped and Co doped ZnO NPs. High intensity of D band (520 nm) in doped NP1 is seen due to higher density of O-vacancy defects. Inset shows low temperature PL spectra of NP2 exhibiting DBEs and AXs indicating presence of free carriers.

$\sim$437 cm^{-1} can be assigned to E2 (high), which is the strongest mode in wurtzite crystal structure. In the doped NP1, E2 (high) is downshifted to 434.0 cm^{-1} and in NP2 it is observed at 436.25 cm^{-1}. This large downshift in NP1 compared to NP2 indicates higher tensile strain in NP1 than that in NP2. Note that XRD analysis showed a compressive strain in the doped NPs. Thus, presence of lattice strain in the doped NPs is confirmed from Raman and XRD analysis. The peaks at 330 and 379 cm^{-1} are assigned to the second-order vibration mode and A1 (TO) mode, respectively. In the doped NPs, the broad peak at $\sim$574 cm^{-1} is deconvoluted into two peaks, as shown in inset of Fig. 3. The peak at 574 cm^{-1} is the E1(LO) mode and can be attributed to defects due to O vacancies, Zn interstitial defect states.[27] Compared with the undoped ZnO NPs, additional strong peaks can be observed at $\sim$547 and $\sim$574 cm^{-1} in the Raman spectra of the $Zn_{1-x}Co_xO$ (x=0.03,0.05). Wang et al..[24] and Cheng et al.[28] also observed this mode in (Co, Al) and Ce-doped ZnO. According to the literature, this mode is induced by host lattice defects, such as oxygen vacancies and Zn interstitials. With the doping content, the host lattice defects in ZnO are activated and amplified and then this mode appears. In the present case, due to the smaller ionic radius of Co^{2+} than that of Zn^{2+}, when Co^{2+} was doped into ZnO lattice, more oxygen vacancies and Zn interstitials are created. Therefore, the appearance of 547 and 574 cm^{-1} can be used to characterize Co^{2+} doped into ZnO lattice.[29]

C. Optical absorption and PL studies

Many groups have confirmed that Co atomically substitutes on Zn sites using a variety of optical methods such as x-ray photoelectron spectroscopy[30] and optical absorption.[30,31] The fourfold coordinated ionic radii of Co^{2+} (0.058 nm) and Zn^{2+} (0.06 nm) are very similar and results in a large solubility of Co^{2+} in the ZnO lattice.[32] Evidence for Co substitution in the ZnO lattice can be inferred from optical UV-Vis absorption spectra. The UV-Vis absorption spectrum was used primarily to find possible change in the band

gap. Figures 4(a) and 4(b) show the UV-Vis spectra taken at RT on different doped samples. The change in absorption peak due to doping indicates a change in the band structure. A blueshift is observed in the bandgap energy for the cobalt doped samples compared to the undoped ZnO. Since the NP sizes are larger than excitonic Bohr radius in ZnO, size effect is unlikely to cause the observed blueshift. It is the strain that causes the change in the band structure of doped ZnO. The $sp-d$ exchange between the ZnO band electrons and localized d-electrons associated with the doped Co^{2+} cations may cause the change in such band structure. The interaction leads to corrections in the energy bands.[33]

PL spectroscopy is an effective method to investigate the presence of defects in semiconductors. The PL spectra of the undoped and Co doped ZnO NPs recorded at RT are shown in Fig. 4(c). There are two distinct emission bands in the spectra of the NPs, one peak is in the UV region ($\sim$380 nm) and another broad visible emission at 520 nm due to the intrinsic defect related band (D). As compared to the undoped NP1, the UV emission peak for the doped NP1 is found to be blueshifted and intensity reduced. The $\sim$380 nm peak usually originates from the near band-edge transition of ZnO and is generally attributed to the recombination of free excitons.[34] The blueshift indicates a higher band gap for the doped NP that may be caused by strain[23] since the NP sizes are much above the excitonic Bohr diameter of ZnO. The D band is centered at $\sim$520 nm and it is observed that the D band becomes broader and very intense with doping of Co in ZnO NPs. It is often attributed to the radiative recombination of photogenerated holes with electrons occupying the singly ionized oxygen vacancy (V_o).[35,36] Based on the band structure calculations the visible emission
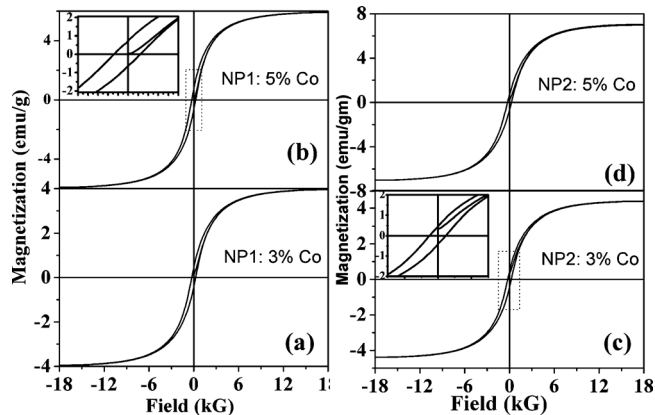
FIG. 5. RT field vs magnetization (M-H) loop showing hysteresis of the Co doped ZnO NPs: (a) 3% Co doped NP1, (b) 5% Co doped and NP1; (c) 3% Co doped NP2, (d) 5% Co doped NP2. The inset shows the magnified M-H loop showing clear ferromagnetic hysteresis behavior. Measured parameters are listed in Table I.

FIG. 6. (Color online) Temperature dependent magnetization (M-T) curve of 3% Co doped ZnO NP1 and NP2 showing high transition temperature (T_c) and sharp ferromagnetic to paramagnetic transition.

has been assigned to V_o and Zn_{in}.[37] Therefore, it is believed that the observed strong visible emission in doped ZnO originates from the deep levels of Co doped ZnO NPs and is due to the presence of V_o and Zn_{in} defects. The inset of Fig. 4(c) shows a PL spectrum of NP2 recorded at low temperature (80 K). The three peaks at 368, 374, and 382 nm are attributed to donor-bound excitons (DBEs), acceptor bound excitons (AXs) and first order phonon replica of AX.[38] Thus low temperature PL measurement shows that the ZnO NPs have free carriers that are important for the FM interaction in DMS materials.

D. Magnetic characterization

The magnetic properties of the Co doped ZnO NPs were investigated using VSM. We observed distinct ferromagnetic behavior at RT in the doped samples only. Despite the presence of some intrinsic defects in undoped ZnO NPs, no trace of FM was observed in the undoped and milled ZnO sample that was first tested under similar conditions using the VSM. This confirms that defects alone in ZnO NPs cannot account for the observed FM in the doped NPs. Figure 5 shows the magnetic hysteresis (M-H) loops for 3% and 5% doped NP1 and NP2 measured at 300 K. The saturation magnetizations (M_s) of the samples varied in the range of 3.95–7.02 emu/g with a coercive filed (H_c) of ~260 G for the 5 h milled sample of different initial particle size and different doping concentration. Samples with higher milling time were also tested by M-H measurement that do not show any significant variation in M_s with milling time indicating that doping is almost saturated for 5 h milling. The change in M_s and H_c for different starting ZnO NPs and doping concentration are compared for NP1 and NP2, as shown in Table I. It is evident that M_s value is higher for Co doped ZnO NP2 with smaller starting sizes of NPs, i.e., NP2 of size 42 nm than NP1 of size 80 nm, and the M_s increases with the doping concentration. Higher M_s in lower size starting nanopowder is likely to be caused by enhanced doping and higher FM ordering in nanometer sized ZnO particles. These results indicate a particle size dependent doping and higher magnetization in na-
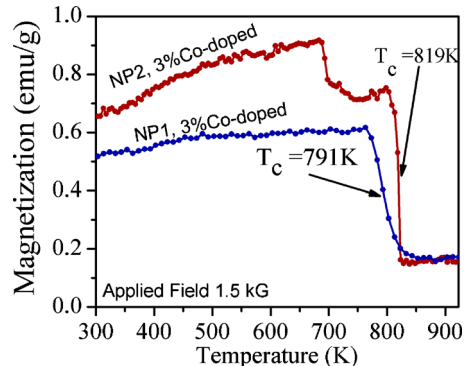
nopowder with lower initial size. Note that ZnO NP2 contains higher concentration of oxygen vacancy defects than the ZnO NP1 (as evident from stronger D band in PL) and these defects mediate the magnetic interactions in the doped NPs. Post growth annealing in air atmosphere at 250 °C affects the magnetization. M_s first increases for 250 °C annealing and then it decreases to a low value for annealing at 500 °C due to paramagnetic transition process (see Table I). Same kind of variation in magnetization can be seen in the magnetization versus temperature (M-T) data shown below where magnetization increases slowly before starting transition toward paramagnetic nature.

It is well known that for use in a wide range of applications without temperature control, the ferromagnet should have a T_c enough above RT (300 K). Figure 6 shows the temperature dependent magnetization of doped NP1 and NP2 in the temperature range 300–850 K. From the differential plot of the M-T curve we obtained the T_c as ~791 K for NP1 and 819 K for NP2 source, which implies that the FM is not due to the Co metal ($T_c > 1300$ K). As seen from the M-T curve, at higher temperature (>700 K) the magnetization shows a rapid decrease with temperature. The magnetization measurement at 300 K of the post M-T measurement, i.e., the Co:ZnO NPs annealed at 850 K in ambient condition shows that the magnetic moment is significantly reduced, which decreases to 0.59 emu/g for the 5% Co doped sample. This magnetic transition suggests that high temperature process causes a rapid destruction of ferromagnetic coupling. Note that compared to the 3% doped samples, 5% doped samples did not exhibit any sharp transition at higher temperature. The absence of a sharp FM to paramagnetic transition in M-T curve for higher doped (5% Co) ZnO NPs may be because of possible antiferromagnetic interaction due to the reduction in average interatomic distance of doped Co ions. Thus, 3% doping of small size NPs is found to yield best result for the observed high temperature FM.

E. Origin of the FM

The origin of observed FM at RT in these NPs could arise from a number of possibilities, such as the intrinsic property of the doped NPs, extended defects in the ZnO NPs, formation of some nanoscale Co-related secondary phase, Co precipitation and CoO. However, CoO phase can be easily

ruled out, since CoO is antiferromagnetic with a Neel temperature of 293 K. Second, metallic Co is also an unlikely source of this FM, as XRD and HRTEM results show no metallic Co clusters in the NPs. Undoped ZnO that were milled under identical conditions does not exhibit any measurable magnetization. Hence, defects alone cannot make the observed high magnetic moment observed in the doped ZnO NPs. Thus, TMs essentially plays the key role to the observed FM. UV-Vis absorption, PL spectra showed a band gap modification which suggests Co^{2+} ions were successfully incorporated into the wurtzite lattice at the Zn^{2+} sites. Therefore FM is expected to arise from the intrinsic exchange interaction of magnetic moments mediated by the defects in doped NPs.

There are several mechanisms proposed in the literature regarding the origin of FM in DMSs. The exact mechanism of intrinsic FM in TM-doped oxides is still under debate. A diversity of theories has been proposed, such as Ruderman-Kittel-Kasuya-Yosida (RKKY) interaction, superexchange, double-exchange between the d states of TMs, free-carrier-mediated exchange, and $sp-d$ exchange mechanism, etc.[39] The RKKY interaction is based on free electrons but ZnO cannot transform into a metal at such a low doping. Direct interactions such as double-exchange or superexchange cannot be responsible for the FM because the magnetic cations are dilute in our samples. All these proposed theories cannot well accord with the experimental results in DMSs.[39] According to the literature, magnetic cations, carriers, and defects can make up bound magnetic polarons (BMPs) that may be responsible for the RT FM. In addition to the magnetic doping effect, oxygen vacancy (V_O) defects have been suggested to play an important role in the magnetic origin for oxide DMSs.[40] The theoretical studies suggest that V_o can cause an obvious change in the band structure of host oxides and makes a significant contribution to the FM.[41,42] The formation of BMPs, which include electrons locally trapped by oxygen vacancy, with the trapped electron occupying an orbital overlapping with the d shells of TM neighbors, has also been proposed to explain the origin of FM.[41] Oxygen vacancies are inherently present in as grown ZnO NPs due to the stabilization of structure. On the basis of observed strong D band emission in PL and intense defect modes seen in Raman spectra, we presume that oxygen vacancies play a key role in the observed FM at RT and above. We notice that post growth air annealing at 250 °C shows increase in M_s owing to the increase in O-vacancy or vacancy clusters that may help to create more BMPs and their percolation.[43] Our systematic study shows that oxygen-vacancy defect constituted BMPs are one of the promising candidate for the origin of room-temperature FM in this system. Within the BMP model, the greater density of oxygen vacancy (V_o) and more doping help to produce more BMPs which yields a greater overall volume occupied by BMPs, leading to the overlap of BMPs and enhancing FM. This evolution is observed in our case, increase in magnetization with the Co concentration indicating that the FM in our samples may be due to percolation of BMPs.

To understand the suitability of the BMP model to explain the observed data, we attempted to fit the M versus H
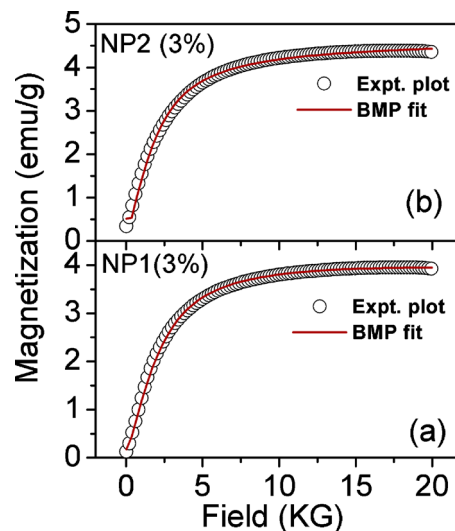

FIG. 7. (Color online) Initial portion of the M-H curve fitted with BMP model [Eq. (1)]: (a) 3% Co doped ZnO NP1 (a) 3% Co doped NP2. Symbols are for experimental data and the solid line is a fit with BMP model. Extracted parameters are shown in Table I.

data to the BMP model by following Chiorescu et al.[44] According to the BMP model, the measured magnetization can be fitted to the relation:

$$M = M_0 L(x) + \chi_m H, \qquad (1)$$

where the first term is from BMP contribution and the second term is due to paramagnetic matrix contribution. Here $M_0 = Nm_s$, N is the number of BMPs involved and m_s is the effective spontaneous moment per BMP. $L(x) = \coth(x) - 1/x$ is the Langevin function with $x = m_{eff}H/(k_B T)$, where m_{eff} is the true spontaneous moment per BMP, and at higher temperature it can be approximated to $m_s = m_{eff}$. We have analyzed the M-H curve by using Eq. (1). The parameters M_0, m_{eff}, and χ_m are variable in the fitting process. The experimental data along with fitted data are shown in Fig. 7 for the 3% Co doped $Zn_{1-x}Co_xO$ sample at 300 K. We notice that the fitted data closely follows the experimental data and the fitted parameters are tabulated in Table I. The total BMP magnetization M_0 values are found to be in the order of 4–7 emu/g. For a given doping concentration, the M_0 values are found to be higher for lower initial size ZnO NPs, i.e., NP2, and this is though to be due to the enhanced doping effect in lower size NPs. Also the M_0 value is found to increase with increase in doping concentration. The paramagnetic susceptibility χ_m is found to be of the order of 10^{-5} cgs unit and its value marginally changes with doping. The spontaneous moment per BMP, m_{eff} is found to be in the order of 10^{-17} emu. By assuming $m_s = m_{eff}$, we have estimated the concentration of BMP, which was found to be in the order of 10^{18} cm^{-3} (see Table I). However, this number is relatively small compared to the concentration necessary for percolation in ZnO. Assuming a realistic value of the effective Bohr radius of the donor orbitals forming the BMPs to be 0.76 nm,[41] the required concentration of BMPs in order to percolate through the ZnO lattice is in the range of 10^{20} cm^{-3} which is two orders of magnitude larger. Thus, the calculated low concentration of BMPs cannot fully account for the observed high

magnetic moment in the doped ZnO. Therefore, BMP model does not satisfactorily explain the observed high temperature FM. Further, the model proposed in Ref. 41 cannot account for such high temperature FM. It was shown that for realistic values of the parameters, the typical Curie temperature is predicted to be in the range of 18 K. In order to have larger Curie temperatures one needs to assume artificially that a substantial amount of the carrier charge density is located on the magnetic impurity site. However, there is no direct experimental evidence to justify such an assumption. Furthermore, it has been shown in theoretical simulations that the strength of the exchange coupling J_{sd} necessary for high temperature FM within the BMP model is about 100 times larger than that the normally assumed value.[45]

Furthermore, in the literature there exists controversy whether the FM observed in oxide DMS could be solely related to intrinsic defects.[10] FM observed in undoped NPs of various oxides such as ZnO, MgO, CeO_2 etc could be a surface phenomenon as proposed by A. Sundaresan and Rao.[11] However, we performed the magnetic characterization of the undoped but 5 h milled ZnO NPs and did not find any measurable hysteresis loop. Note that in the literature, defect related magnetization observed in the undoped NPs is of much lower magnitude (10^{-3} emu/g) as compared to doped DMS.[11] We observed at least three orders of magnitude higher magnetization in the doped ZnO NPs. Thus, it appears that both TMs as well as defects are important ingredients for the magnetic interactions and presence of TM is essential for the high magnetization value observed here. In a recent study, Pemmaraju et al.[45] identified the $Co-V_O$ pair defect as the most likely candidate for the near-RT FM in Co doped ZnO and demonstrated that such center can indeed promote long-range coupling, if additional n-type doping is present. However, the required concentrations of such defects are extremely high and the predicted T_c is also below 300 K.

It may be noted that very few studies have reported such high M_s value at RT in the Co doped ZnO as observed in this study. A majority of the previous studies on Co doping of ZnO shows a relatively smaller M_s value at or above RT. It is likely that due to large density of point defects as well as extended defects such as dislocations associated with the strain in the ZnO lattice, magnetic interactions mediated by the interaction of Co and defects is enhanced in the doped NPs. It is expected that samples with higher concentration of defects/strain would show higher magnetization. However, we notice higher magnetization in samples with lower strain. Thus, high magnetization may not be directly correlated with the lattice strain in the doped ZnO NPs.

It is worth mentioning that recent consensus in the literature on Co doped ZnO has clearly drifted toward the conclusion that one cannot get carrier mediated FM in bulk or single crystal thin film ZnCoO samples even with a relatively large concentration of n-type carriers.[46] The presence of extended structural defects such as grain boundaries is now widely regarded as a necessity to observe signatures of high temperature FM.[47] Xing et al.[48] suggested that structural inhomogeneity can boost the RT FM by promoting the formation of BMPs in Cu doped ZnO nanowires. From the experimental data, we found that doped NPs have substantial lattice strain. In the ball milled NPs, lattice strain is usually caused by screw type dislocations that develop during milling.[49] Usually, this dislocation density first goes up with milling time and then it reduces with further milling associated by particle size reduction. In a previous study, we have shown from HRTEM that ball milled ZnO NPs possessed considerable lattice strain[23] and this may caused by dislocations in the nanocrystals. Thus, the dislocations or grain boundary can contribute to the observed FM. Similar proposal has been made by Hsu et al.[47] and Podila et al.[9] However, more studies would be required to pinpoint the origin of high temperature FM.

IV. CONCLUSION

In summary, nanocrystalline ZnCoO has been synthesized by a simple ball milling method using two different initial sizes of ZnO NPs. Microstructure analysis shows that the NPs are of single crystalline ZnO wurtzite structure. XRD, HRTEM, EDS, UV-Vis absorption measurements indicate that Co^{2+} substitute into ZnO lattice at Zn^{2+} site. Raman scattering and PL studies confirm the presence of large amount strain and defects, respectively, in the doped NPs. We found that BMP model fitting to experimental M-H data leads to a low concentration of BMPs to give rise to large M_s value. Though the exact mechanism for the observed FM is not clear, possible pairing of the Co^{2+} and extended defect (e.g., dislocations) may be responsible for the observed FM at and above RT. As compared to the Co doping of bulk and thin film of ZnO, ZnO NPs exhibit enhanced ferromagnetic exchange interaction perhaps related to the weak confinement/size effect. We have found that ZnO NPs of smaller initial size show higher M_s value. In this work, RT FM have been obtained in Co doped ZnO DMSs material and it's Curie temperature (T_c) 800 K is much above RT. It is considered to be an important step for the development of semiconductor devices that can retain their FM properties above RT for the realization of practical commercial or mobile devices.

[1]S. J. Pearton, C. R. Abernathy, D. P. Norton, A. F. Hebard, Y. D. Park, L. A. Boatner, and J. D. Budai, Mater. Sci. Eng. R. **40**, 137 (2003).
[2]H. Ohno, Science **281**, 951 (1998).
[3]T. Dietl, H. Ohno, F. Matsukura, J. Cibert, and D. Ferrand, Science **287**, 1019 (2000).
[4]Y. Matsumoto, M. Murakami, T. Shono, T. Hasegawa, T. Fukumura, M. Kawasaki, P. Ahmet, T. Chikyow, S. Koshihara, and H. Koinuma, Science **291**, 854 (2001).
[5]P. Sharma, A. Gupta, K. V. Rao, F. J. Owens, R. Sharma, R. Ahuja, J. M. O. Guillen, B. Johansson, and G. A. Gehring, Nature Mater. **2**, 673 (2003).
[6]S. A. Wolf, D. D. Awschalom, R. A. Buhrman, J. M. Daughton, S. Von Molnar, M. L. Roukes, A. Y. Chtchelkanova, and D. M. Treger, Science **294**, 1488 (2001).
[7]T. Dietl, Semicond. Sci. Technol. **17**, 377 (2002).
[8]S. J. Pearton, D. P. Norton, K. Ip, Y. W. Heo, and T. Steiner, Superlattices

Microstruct. **34**, 3 (2003).

[9]R. Podila, W. Queen, A. Nath, J. T. Arantes, A. L. Schoenhalz, A. Fazzio, G. M. Dalpian, J. He, S. J. Hwu, M. J. Skove, and A. M. Rao, Nano Lett., **10**, 1383 (2010).

[10]J. M. D. Coey and S. A. Chambers, MRS Bull. **33**, 1053 (2008).

[11]A. Sundaresan and C. N. R. Rao, Nano Today **4**, 96 (2009).

[12]T. Fukumura, Y. Yamada, H. Toyosaki, T. Hasegawa, H. Koinuma, and M. Kawasaki, Appl. Surf. Sci. **223**, 62 (2004).

[13]S. B. Ogale, Adv. Mater. **22**, 3125 (2010).

[14]S. A. Chambers, T. Droubay, C. M. Wang, A. S. Lea, R. F. C. Farrow, L. Folks, V. Deline, and S. Anders, Appl. Phys. Lett. **82**, 1257 (2003).

[15]Y. Zou, Z. Qua, J. Fang, and Y. Zhang, J. Magn. Magn. Mater. **321**, 3352 (2009).

[16]J. Iqbal, B. Wang, X. Liu, D. Yu, B. He, and R. Yu, New J. Phys. **11**, 063009 (2009).

[17]S. Ghoshal and P. S. Anil Kumar, J. Magn. Magn. Mater. **320**, L93 (2008).

[18]K. Ueda, H. Tabata, and T. Kawai, Appl. Phys. Lett. **79**, 988 (2001).

[19]C. Song, F. Zeng, K. W. Geng, X. B. Wang, Y. X. Shen, and F. Pan, J. Magn. Magn. Mater. **309**, 25 (2007).

[20]S. Deka, R. Paricha, and P. A. Joy, Chem. Mater. **16**, 1168 (2004).

[21]O. D. Jayakumar, I. K. Gopalakrishnan, C. Sudakar, R. M. Kadam, and S. K. Kulshreshtha, J. Alloys Compd. **438**, 258 (2007).

[22]C. N. R. Rao and F. L. Deepak, J. Mater. Chem. **15**, 573 (2005).

[23]P. K. Giri, S. Bhattacharyya, D. K. Singh, R. Kesavamoorthy, B. K. Panigrahi, and K.G. M. Nair, J. Appl. Phys. **102**, 093515 (2007).

[24]J. B. Wang, G. J. Huang, X. L. Zhong, L. Z. Sun, Y. C. Zhou, and E. H. Liu, Appl. Phys. Lett. **88**, 252502 (2006).

[25]K. Samanta, P. Bhattacharya, R. S. Katiyar, W. Iwamoto, P. G. Pagliuso, and C. Rettori, Phys. Rev. B **73**, 245213 (2006).

[26]D. G. Mead and G. R. Wilkinson, J. Raman Spectrosc. **6**, 123 (1977).

[27]J. Alaria, H. Bieber, S. Colis, G. Schmerber, and A. Dinia, Appl. Phys. Lett. **88**, 112503 (2006).

[28]B. C. Cheng, Y. H. Xiao, G. S. Wu, and L. D. Zhang, Appl. Phys. Lett. **84**, 416 (2004).

[29]L. B. Duan, G. H. Rao, Y. C. Wang, J. Yu, and T. Wang, J. Appl. Phys. **104**, 013909 (2008).

[30]A. C. Tuan, J. D. Bryan, A. B. Pakhomov, V. Shutthanandan, S. Thevuthasan, D. E. McCready, D. Gaspar, M. H. Engelhard, J. W. Rogers, Jr., K. Krishnan, D. R. Gamelin, and S. A. Chambers, Phys. Rev. B **70**, 054424 (2004).

[31]K. Samanta, P. Bhattacharya, and R. S. Katiyar, Appl. Phys. Lett. **87**, 101903 (2005).

[32]Z. Jin, M. Murakami, T. Fukumura, Y. Matsumoto, A. Ohtomo, M. Kawasaki, and H.Koinuma, J. Cryst. Growth **214–215**, 55 (2000).

[33]S. Guha, K. Ghosh, J. G. Keeth, S. B. Ogale, S. R. Shinde, J. R. Simpson, H. D. Drew, and T. Venkatesan, Appl. Phys. Lett. **83**, 16 (2003).

[34]C. Li, G. Fang, Q. Fu, F. Su, G. Li, X. Wu, and X. J. Zhao, J. Cryst. Growth **292**, 19 (2006).

[35]H. T. Ng, B. Chen, J. Li, J. Han, M. Meyyappan, J. Wu, S. X. Li, and E. E. Haller, Appl. Phys. Lett. **82**, 2023 (2003).

[36]C. W. Cheng, G. Y. Xu, H. Q. Zhang, and Y. Luo, Mater. Lett. **62**, 1617 (2008).

[37]X. Liu, X. Wu, H. Cao, and R. P. H. Chang, J. Appl. Phys. **95**, 3141 (2004).

[38]V. A. Fonoberov, K. A. Alim, A. A. Balandin, F. Xiu, and J. Liu, Phys. Rev. B **73**, 165317 (2006).

[39]S. J. Pearton, W. H. Heo, M. Ivill, D. P. Norton, and T. Steiner, Semicond. Sci. Technol. **19**, R59 (2004).

[40]H. S. Hsu, J. C. A. Huang, Y. H. Huang, Y. F. Liao, M. Z. Lin, C. H. Lee, J. F. Lee, S. F. Chen, L. Y. Lai, and C. P. Liu, Appl. Phys. Lett. **88**, 242507 (2006).

[41]J. M. D. Coey, M. Venkatesan, and C. B. Fitzgerald, Nature Mater. **4**, 173 (2005).

[42]J. E. Jaffe, T. C. Droubay, and A. A. Chambers, J. Appl. Phys. **97**, 073908 (2005).

[43]K. R. Kittilstved, N. S. Norberg, and D. R. Gamelin, Phys. Rev. Lett. **94**, 147209 (2005).

[44]C. Chiorescu, J. L. Cohin, and J. J. Neumeier, Phys. Rev. B **76**, 020404(R) (2007).

[45]C. D. Pemmaraju, R. Hanafin, T. Archer, H. B. Braun, and S. Sanvito, Phys. Rev. B **78**, 054428 (2008).

[46]T. C. Kaspar, T. Droubay, S. M. Heald, P. Nachimuthu, C. M. Wang, V. Shutthanandan, C. A. Johnson, D. R. Gamelin, and S. A. Chambers, New J. Phys. **10**, 055010 (2008).

[47]H. S. Hsu, J. C. A. Huang, S. F. Chen, and C. P. Liu, Appl. Phys. Lett. **90**, 102506 (2007).

[48]G. Z. Xing, J. B. Yi, J. G. Tao, T. Liu, L. M. Wong, Z. Zhang, G. Ping Li, S. J. Wang, J. Ding, T. C. Sum, C. H. A. Huan, and T. Wu, Adv. Mater. **20**, 3521 (2008).

[49]P. K. Giri, J. Phys. D: Appl. Phys. **42**, 245402 (2009).